ADVANCED FUNCTIONAL MATERIALS
www.afm-journal.de

Microrobots Derived from Variety Plant Pollen Grains for Efficient Environmental Clean Up and as an Anti-Cancer Drug Carrier

*Tijana Maric, Muhammad Zafir Mohamad Nasir, Nur Farhanah Rosli, Maja Budanović, Richard D. Webster, Nam-Joon Cho, and Martin Pumera**

The production of large quantities of micromachines and microrobots is limited by fabrication methods and the use of synthetic templates. Pollen is one of the most stable structures in the world, capable of surviving harsh treatment and for millions of years. Pollen grains are available in large variety of shapes and sizes. The use of a wide variety of naturally abundant, nontoxic pollen grains for the efficient fabrication of platinum-pollen (Pt-pollen) hybrid microrobots capable of fast propulsion for environmental and biomedical applications is demonstrated. Nine different pollen grains are selected and modified (dandelion, pine, lotus, sunflower, poppy, camellia, lycopodium, cattail, and galla) to demonstrate the robustness of different types of pollen grains for potential applications in environmental remediation. The efficient mobility rendered by the fabricated microrobots enhances their performance in the removal of heavy metals in aqueous medium. Furthermore, they can be used as doxorubicin carriers.

1. Introduction

The main goal of nanotechnology is successful replacement of macroscopic vehicles with miniaturized devices—micro/nanorobots that can perform similar or improved varied functions in environmental science and biomedical applications.[1,2] Self-propelling autonomous nano/microrobots have garnered significant interest not only in nanotechnology but in other spectra of science also, such as medicine.[3–7] These self-propelling miniaturized devices are able to drive by the following mechanisms: self-electrophoresis, bubbles propulsion, self-diffusion phoresis, and Marangoni effect.[8–10] Small size and fast velocities of microrobots have been favorable properties serving as highly efficient platforms for water clean-up in the removal of heavy metals,[11,12] oils,[13,14] dyes,[15] chemical warfare agents,[16] phenolic pollutants,[17] pollutants degradation,[1,18] and pathogens.[19] Recent efforts have also demonstrated wide range of biomedical application of microrobots as drug carriers,[20] cargo delivery,[21,22] nanosurgery,[23] and cancer therapy.[24–26]

Previously, pollen grains have gained increasing attention due to their environmentally friendly properties, structural stability, biocompatibility, and monodispersity.[27–34] The exine (outer layer) is composed of a biologically and chemically resistant crosslinked biopolymer called sporopollenin, which is considered the diamond of biopolymers and exhibits remarkable mechanical stability even compared to many carbon types and synthetic polymers from which micromotors are typically fabricated.[27,28,35] In contrast, intine (inner layer) is made up of pectin, cellulose, proteins, and polysaccharides. Additionally, the hollow internal shells of pollen grains make them suitable

T. Maric, Dr. M. Z. M. Nasir, N. F. Rosli, Dr. M. Budanovic, Prof. R. D. Webster
Division of Chemistry & Biological Chemistry
School of Physical and Mathematical Sciences
Nanyang Technological University
Singapore 637371, Singapore

Prof. N.-J. Cho
School of Materials Science and Engineering
Nanyang Technological University
Singapore 637459, Singapore

Prof. M. Pumera
Center for Advanced Functional Nanorobots
Department of Inorganic Chemistry
Faculty of Chemical Technology
University of Chemistry and Technology Prague
Technická 5, Prague 6 166 28, Czech Republic
E-mail: martin.pumera@vscht.cz

The ORCID identification number(s) for the author(s) of this article can be found under https://doi.org/10.1002/adfm.202000112.

DOI: 10.1002/adfm.202000112

Prof. M. Pumera
Department of Chemical and Biomolecular Engineering
Yonsei University
50 Yonsei-ro, Seodaemun-gu, Seoul 03722, Korea

Prof. M. Pumera
Department of Medical Research
China Medical University Hospital
China Medical University
No. 91 Hsueh-Shih Road, Taichung 404, Taiwan

Prof. M. Pumera
Future Energy and Innovation Laboratory
Central European Institute of Technology
Brno University of Technology
Purkyňova 656/123, Brno CZ-616 00, Czech Republic

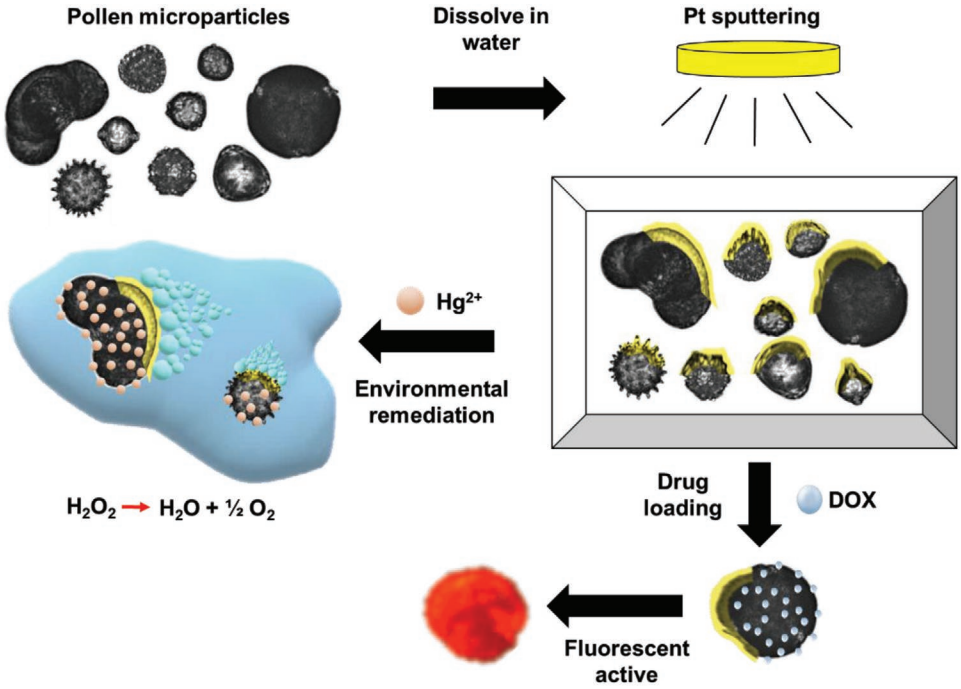

Scheme 1. Schematic representation on the fabrication of Pt-pollen microrobots. The fabricated microrobots were subsequently used for removal of Hg^{2+} ions in aqueous solution and loaded with anti-cancer drug (Doxorubicin).

candidates as microencapsulant to store and deliver cargo. Cho et al. recently reported extraction methods of dandelion sporopollenin exine capsules which potentially can find applications in drug delivery as well as food industry.[36,37] Additionally, pine pollen grains were loaded with bovine serum albumin for targeted oral delivery. The triple cavity structure of the pollen grains allowed for excellent loading.[38] Similarly, *Lycopodium clavatum* spores were reported to display efficient encapsulation of 5-fluorouracil and release in gastric environment.[39]

Herein, we demonstrate a template-free approach by fabricating microrobots based on pollen grains which exhibit self-propulsion movement by bubbles formation due to the decomposition of hydrogen peroxide (H_2O_2) by platinum. Recently, we have demonstrated sunflower pollen grain microrobots,[40] however, the study was limited to one grain size and structure. It is important to note that there is a great variety of pollen sizes, shapes, and surface structure and we decided to investigate these. Herein, we have fabricated hybrid inorganic-biomaterials microrobots from nine different types of pollen grains (dandelion, pine, lotus, sunflower, poppy, camellia, lycopodium, cattail, and galla) asymmetrically sputtered with a thin layer of platinum. The fabricated platinum-pollen (Pt-pollen) microrobots were studied by investigating their applications for heavy metals removal (Hg^{2+}) in aqueous medium and anti-cancer drug attachment.

2. Results and Discussion

Nine different types of the pollen grains were studied (dandelion, pine, lotus, sunflower, poppy, camellia, lycopodium, cattail, and galla) for the fabrication of autonomously moving Pt-pollen microrobots. These pollen grains were chosen due to their natural abundancy, great efficiency, and reproducibility for microrobots preparation.[40] **Scheme 1** provides an illustration on the procedures for Pt-pollen microrobots preparation as well as proof-of-concept applications in Hg^{2+} ions removal in aqueous solution and anti-cancer drug loading. In summary, pollen grains serve as structural templates for microrobots fabrication. A thin layer of platinum was asymmetrically sputtered onto one side which functions as catalyst for the decomposition of hydrogen peroxide (H_2O_2) and formation of bubbles for propulsion of the fabricated microrobots. It should be noted that we previously introduced MnO_2 or Ag to this field; however, we chose platinum due to its stronger catalytic ability toward fuel decomposition and thus stronger power output and high microrobots velocities.[41]

The comprehensive procedure for Pt-pollen microrobots preparation is further elaborated in Experimental Section. Characterization studies were first performed to understand the unique morphological structural features of the selected pollen grains and their corresponding fabricated micromotors counterparts. To examine the differences in particle sizes, shapes, and features with their respective microrobots counterparts, scanning electron microscopy (SEM), dynamic imaging particle analysis (DIPA), and energy-dispersive X-ray spectroscopy (EDS) were carried out. SEM was first performed to understand and analyze the contrasting microscopic surface features of the selected pollen grains (**Figure 1**). It is postulated that specific surface morphologies and characteristics would affect potential applications of the fabricated Pt-pollen microrobots. From Figure 1, it is apparent that each type of plant pollen has uniform size distribution and porous surfaces. Based on the SEM images obtained, the different pollen grains can be broadly categorized based on their common shapes or structural features. Lotus,

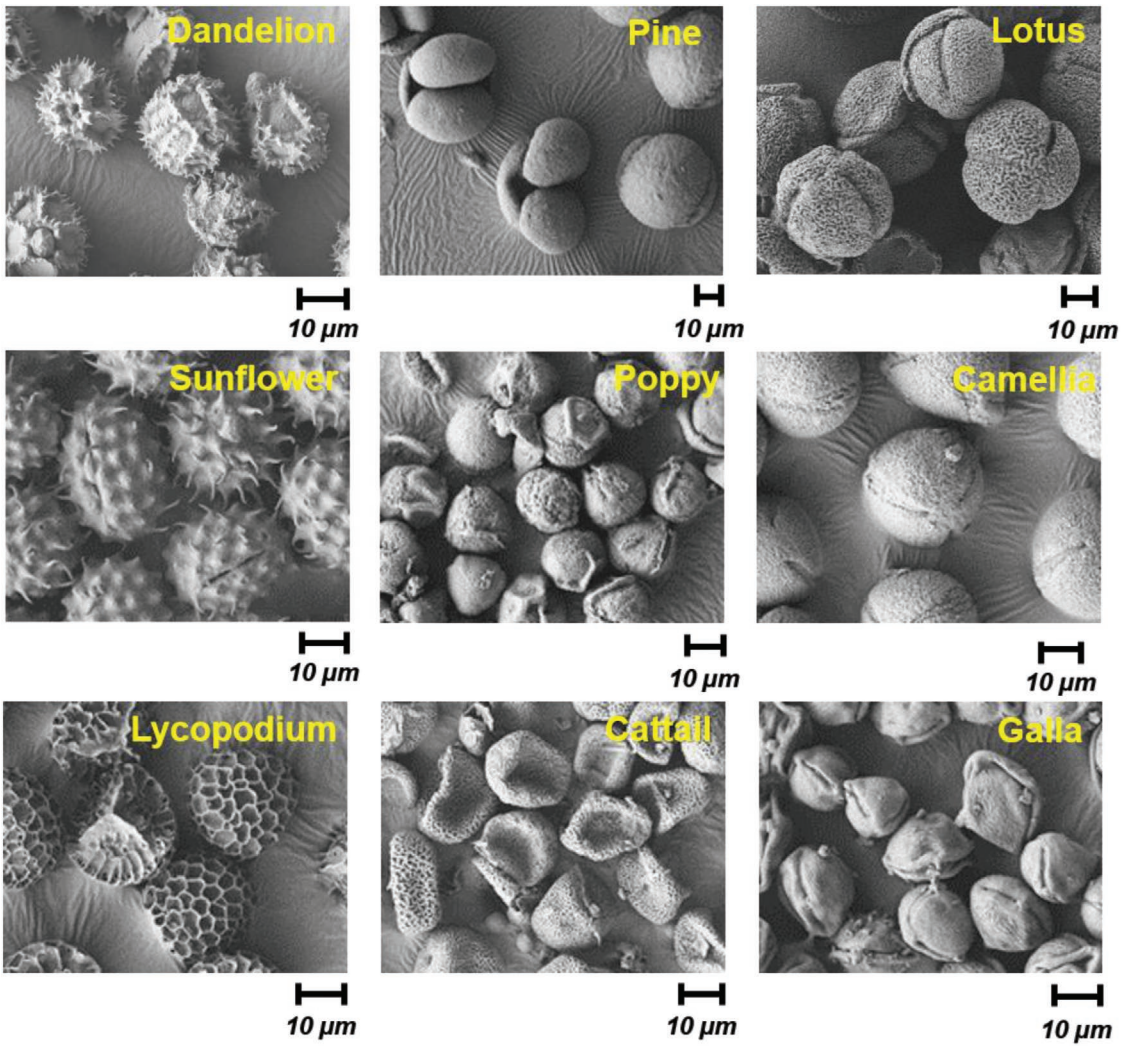

Figure 1. SEM images of nine different types of bare plant pollens. Scales as indicated in respective images.

sunflower, and camellia have spherical shape; pine, poppy, galla, cattail, and dandelion can be classified into a group of pollen grains which has oblate shape as they have ratio between the length of the polar and equatorial axis less than 1. In contrast, lycopodium has ratio higher than 1 and it has defined prolate shape. Depending on the apertures, lotus, camellia, poppy, and galla exhibit colpus structure with elliptical or rectangular aperture with length at least twice times longer than width. Dandelion, sunflower, lycopodium, and cattail have pore structure with small apertures on their surface. In particular, pine pollen grains have the distinctive "Mickey Mouse" leptomate structure where the middle portion resembles the head attached to two ears on both sides (air sacs). In the case of lycopodium pollen, it is very well defined by many open chambers.[42] The trend in pore characteristics is also consistent with results obtained in past Brunauer–Emmett–Teller isotherm experiments and correlations with SEM-based pore analysis.[38] These apparent differences in structural features could play prominent roles in the mobility and performances in potential applications of the fabricated microrobots which will be further discussed.

Following SEM morphological structure characterization, we studied DIPA to ascertain respective pollens sizes and shapes (**Figure 2**). High-resolution camera (FlowCam) was used to obtain size distribution for each type of pollen by analyzing 500 individual pollen grains. From Figure 2, each graph consists of histogram data and respective fitted Gaussian curves of each pollen grain's diameter size as a function of frequency. The selected pollen grains were found to exist within a broad size range distribution with pine pollen grains having the biggest diameter (≈62 μm) while cattail pollen grains having the smallest diameters (≈22 μm). Presently, extensive studies have been directed toward exploring and analyzing of self-propulsion of microrobots. In this part, owing to their different morphologies, we set forth to investigate the mobilities of the different fabricated Pt-pollen microrobots by performing comparative velocity experiments. The experiments were conducted in solutions containing 1 wt% sodium dodecyl sulfate (SDS) at two different concentrations of H_2O_2 (3 and 5 wt%). All prepared microrobots [Pt-dandelion (Pt-Dan), Pt-pine, Pt-lotus (Pt-Lot), Pt-sunflower (Pt-Sun), Pt-poppy (Pt-Pop), Pt-camellia (Pt-Cam),

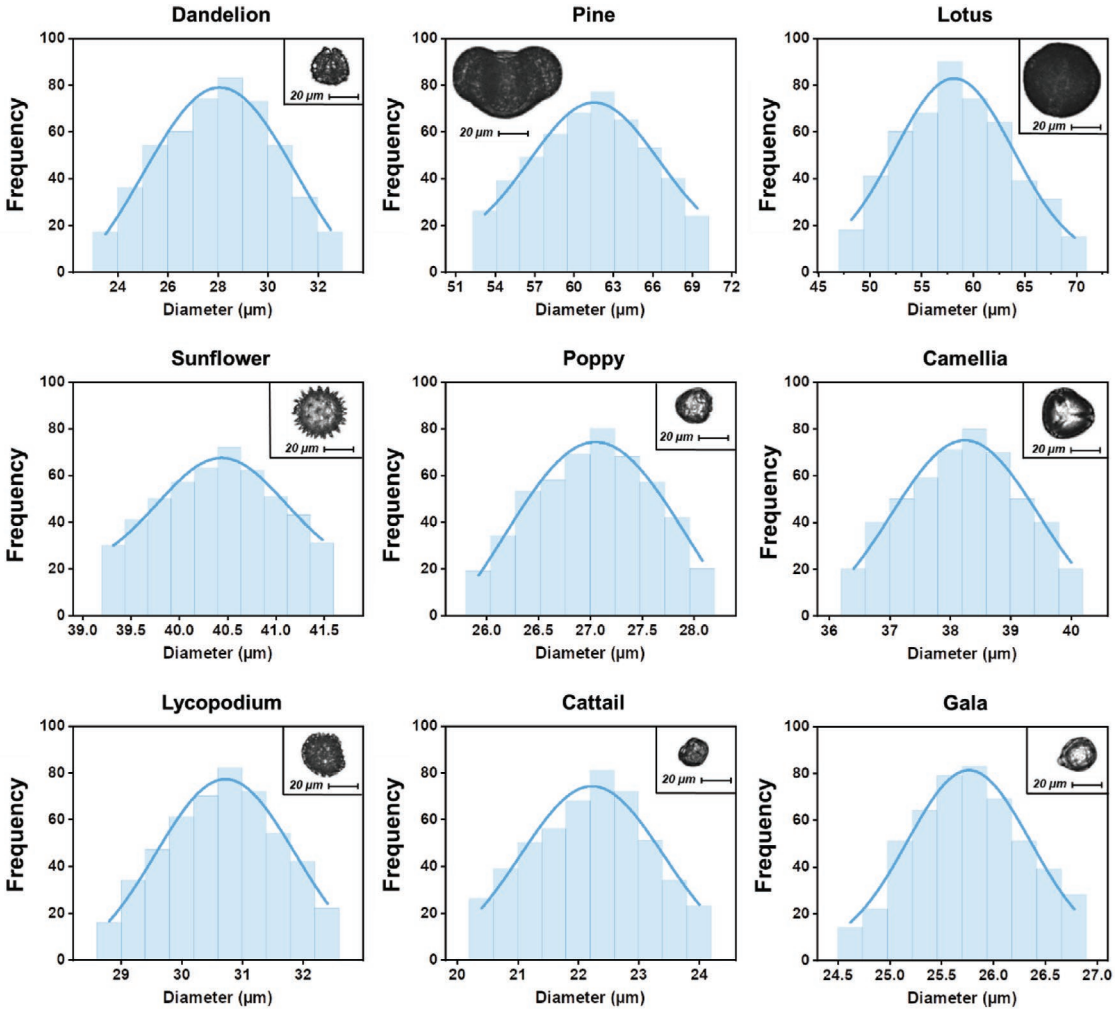

Figure 2. Diameter analysis performed by DIPA obtained from three independent measurements. Each graph presents a function of diameter versus frequency. Scales as indicated in respective images.

Pt-lycopodium (Pt-Lyc), Pt-cattail (Pt-Cat), and Pt-galla (Pt-Gal)] exhibited higher average velocities in 5 wt% H_2O_2 compared to 3 wt% H_2O_2 as predicted (**Figure 3**A). Higher concentrations of H_2O_2 increase O_2 saturation levels which promotes nucleation rates thus resulting in faster velocities.[43]

Comparing the velocities, the fabricated microrobots were found to move with average velocities of >50 μm s^{-1} in 3 wt% H_2O_2 which significantly increased (>140 μm s^{-1}) in 5 wt% H_2O_2. All presented average values with their respective standard deviations were calculated from 20 individual microrobots velocities. Pt-Cat microrobots were found to exhibit the slowest average velocity (49.9 ± 9.5 μm s^{-1} for 3 wt% H_2O_2 and 137.2 ± 25.8 μm s^{-1} in 5 wt% H_2O_2) while Pt-Lot microrobots have the fastest average velocity (217.0 ± 36.7 μm s^{-1} in 3 wt% of H_2O_2 and 349.9 ± 44.2 μm s^{-1} in 5 wt% of H_2O_2). Additionally, motion trajectories of the respective fabricated Pt-pollen microrobots in 3 wt% H_2O_2 for duration of 2 s were monitored (Figure 3B). It was noted that most of the Pt-pollen microrobots were propelled in circular motion trajectories with the exception of Pt-Lot and Pt-Gal microrobots which moved around their respective rotation axes. Microrobots which had faster average velocities made bigger circumferences hence they generated greater displacements for the same time interval. It is important to note that Pt-pollen microrobots cannot move in the absence of both SDS and H_2O_2.

The microrobots were able to propel by bubbles generation followed by bubbles detachment at the sputtered Pt surface. Taking into account the fact that bubbles generation is dependent on the microrobots' geometries and shapes, the average velocities obtained are in accordance with theory. Zhao et al. previously performed kinetics studies of Janus particles and discovered that particles with diameters <10 μm could not be easily propelled by bubbles formation.[44] Bubbles nucleation can occur when microrobots in aqueous solution accumulate oxygen gas which reach heterogenous nucleation energy (critical energy).[45] It depends on the irregularity on the surface of microrobots as well as O_2 saturation concentration. From SEM images captured (Figure 1), the different shapes and geometries of pollen microrobots were presented which are different from Janus and tubular microrobots reported. As such, the surface area and coverage of Pt sputtered surface changes accordingly. Pt-Lot and Pt-Dan microrobots have

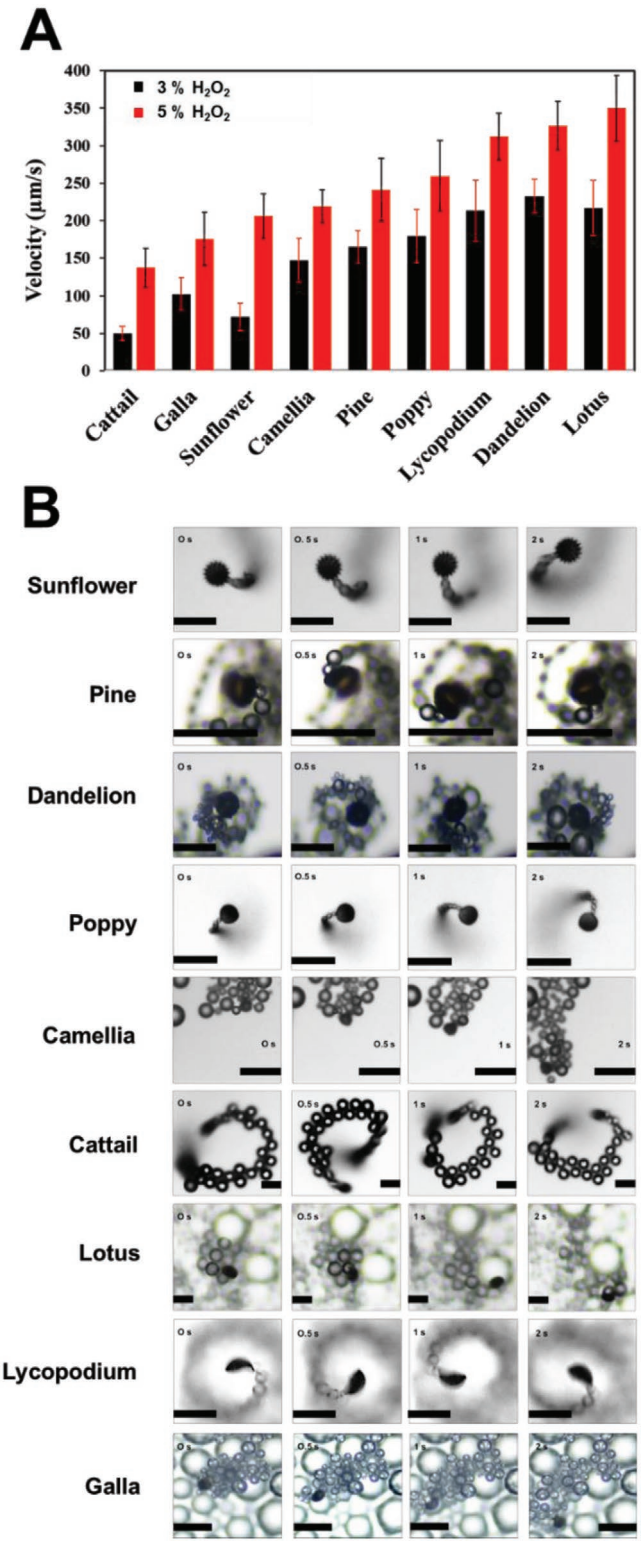

Figure 3. A) Dependencies of average velocities of Pt-pollen microrobots in respective H_2O_2 concentrations. Average velocities and standard deviations at respective H_2O_2 concentrations were obtained from 20 independent measurements. B) Motion trajectories of respective Pt-pollen microrobots in 3 wt% H_2O_2 over duration of 2 s. Scale bars represent 50 μm for each image.

concave-like surfaces which require lesser energy to form bubbles. Thus, they display faster velocities. On the other hand, Pt-Cat and Pt-Gal microrobots have convex-like shapes. Hence, more energy would be required to generate bubbles.[46] These can be explained from the fact that free energy of bubbles generation for convex and concave surfaces is different (concave surface ≈ 0). Additionally, any contamination or defects during fabrication of microrobots can change contact angles, which reduces the efficiency of nucleation. Previously, it was shown that Pt-Sun microrobots generate bubbles between the spikes and that nucleation depends on the gaps between the spikes.[40] Velocity of Pt-pollen microrobots can be explained by Stokes's law extended to nonspherical particles.[47] Microrobots propulsion depends on both driving force and drag force in the aqueous medium. Drag forces on Pt-pollen microrobots can be obtained from the following equation

$$F_D = 3\pi\eta\, V d_v K \tag{1}$$

where η is the dynamic viscosity, V is the velocity of nonspherical particle, d_v is the diameter of the spherical object, K is the corrected shape coefficient (can be defined for any shape)

$$K = \frac{V_s}{V} \tag{2}$$

where V_s is the velocity of the sphere with the same diameter to the diameter of nonspherical particle.

Shape coefficient is larger than 1 for irregular shape microrobots, compared to spherical Janus microrobots (shape coefficient = 1). It can be interpreted as the velocity of the Pt-pollen microrobots being less than velocity of the equivalent sphere. Camellia and sunflower can be good example for this explanation as sunflower pollen grain has very similar diameter to the diameter of spherical particle (camellia pollen grain). Therefore, camellia pollen grains have shape coefficient $K \approx 1$, and shape coefficient of sunflower pollen grains, due to the spikes presented on the surface, is ≈1.18. Taking into account this assumption, it is expected that Pt-Cam move with higher velocity than Pt-Sun microrobots which is in correlation with experimental results. From Equation (1), microrobots with irregular shape have larger value for drug force compared to spherical microrobots. Escarpa et al. previously reported that outer surface microrobots roughness increases drag force on them and therefore reduces their velocities.[48]

Scrutinizing further, we evaluated the potential application of fabricated Pt-pollen microrobots for Hg^{2+} removal in aqueous medium. Neustadt and Pieczenik reported that Hg^{2+} overdose could cause serious health problem such as autoimmune diseases, memory loss, insomnia, and anxiety.[49] Water polluted with heavy metals is considered wastewater and presents a global problem for humanity even in very small concentrations.[50] The lack of potable water, coupled with the increasing pollution of water bodies generates an increasing global demand for clean water. This need has attracted the attention of many scientific institutions and industries with aims to develop efficient and economical wastewater treatment technologies to meet the increasing demand. Adsorption technique is widely adopted due to its simplicity, easy performance, and the potential use

of cheaper alternative adsorbent materials. Previously, naturally available halloysite[51,52] were used as microrobots template and displayed efficient performance in the removal of heavy metals in wastewater. The basic parameters and properties considered in the selection of adsorbents for purifying contaminated water include selectivity, high adsorption capacity, abundancy, simplicity of synthesis and modification, low cost, and regeneration possibility. Natural pollen grains, in addition to being cheap and abundant, can also be promising micromaterials for removing Hg^{2+} ions in contaminated water. Pt-pollen microrobots are more efficient mobile adsorbents for fast Hg^{2+} ions removal compared to bare pollen grains due to enhanced assisted fluid mixing attributed to microrobots' mobility.[40] For this purpose, Pt-pollen microrobots were exposed to aqueous solutions containing 1 ppm Hg^{2+}.

Figure 4A compares the Hg^{2+} removal performance of Pt-pollen microrobots (black bars) and their corresponding bare pollen grains (red bars). First, the respective microrobots were exposed to 1 ppm Hg^{2+} for different durations of 1, 5, 30, and 120 min. All graphs are displayed as a percentage of Hg^{2+} removal over exposure time durations (0–120 min). From Figure 4A, most prepared microrobots showed more efficient removal of Hg^{2+} compared to their respective bare pollen grains except Pt-Lot, Pt-Pine, and Pt-Gal microrobots. These microrobots did not show much difference in adsorption performance compared to their corresponding pollen grains. Pt-Lot microrobots have very large surface area and propelled with the fastest velocities. These factors could have attributed to the highly efficient removal of Hg^{2+} by Pt-Lot microrobots. Despite the fact, Pt-Lot microrobots did not show much difference in adsorption performance compared to their corresponding pollen grains which could be justified by very good adsorption capability of bare material (lotus pollen grain) so that additional propulsion does not have much influence on adsorption performance.

Pt-Gal microrobots exhibit the slowest velocities and they exist as small particles. As such, the slow propelling Pt-Gal microrobots do not show enhanced adsorption performance compared to bare galla pollen grains. Comparing the performances at exposure time of 1 min to their respective bare pollen grains, it was observed that removal of Hg^{2+} by Pt-Dan microrobots (37%) showed greatest enhancement than to bare dandelion pollen grains (12%). The dynamic and robust propulsion motion, coupled with the fast velocity and good adsorption capabilities, could have resulted in such improved performance.

Figure 4B provides a comparison on the removal efficiency of Hg^{2+} by the fabricated microrobots over duration of 120 min. All graphs depict increasing trend for the removal of Hg^{2+} over the experimental duration and reached maximum removal percentage after 120 min. Pt-Lyc and Pt-Cat microrobots reached the highest Hg^{2+} removal efficiency of ≈90%. The high adsorption efficiency 120 min after exposure to Hg^{2+} could be attributed to the availability of high surface area on the unsputtered pollen surface for adsorption to occur. The most efficient microrobot for the removal of Hg^{2+} in aqueous medium was found to be Pt-Lyc which displayed high removal percentages throughout all analysis durations while the least efficient microrobot was Pt-Pin which displayed the lowest percentages throughout the experimental duration. It is important to note that adsorption performance is not only governed by size of microrobots. Adsorption capacity depends on surface functionalities such as surface charge, amount of active sites, and available surface area on the microrobots as adsorbents. Pt-Pin microrobots have the largest surface area but likely they do not have contain large amount binding sites available for adsorption which results in a lower adsorption capacity. Pine pollen grain is only studied pollen grain which contains corpus and two saccus (bi-saccate), the rest are mono-compartmental as they consist of only one corpus. This unique structure of pine pollen grains opens the possibility that Hg^{2+} ions can load only into the exine of the porous central cavity which is water permeable, but not into the nonporous air-sac.[53] Nonetheless, all fabricated microrobots displayed good performances with high removal pollutants percentages.

EDS elemental mapping characterization was performed (**Figure 5**) to confirm the adsorption of Hg^{2+} onto the microrobots and verify the results obtained. It can be deduced that Pt layer was sputtered and Hg^{2+} presence did not perturb the natural structures of the pollen grains for each fabricated microrobots (SEM images, Figure 5). Additionally, the elemental mappings obtained displayed the presence of Hg on all fabricated microrobots which strongly suggests the adsorption of the ions onto the surface of the microrobots after 120 min.

Next, average velocity measurements were performed in the presence of 1 ppm Hg^{2+} for exposure duration of 30 min (**Figure 6**). Time $t = 0$ for each graph represents the average velocities of each fabricated Pt-pollen microrobots in the absence of Hg^{2+}. The mobility of the Pt-Dan microrobots was found to significantly decrease even after only 1 min exposure time. The presence of Hg^{2+} had the least impact on Pt-pollen microrobots after 1 min exposure time (velocity dropped by 58% from initial value). In contrast, velocities of Pt-Gal, Pt-Lyc, Pt-Cam, and Pt-pollen microrobots decreased significantly (>85%) for the same exposure time. It was also interesting to note that Pt-Cat and Pt-Gal microrobots ceased motion after 30 min exposure time. Pt-Cat microrobots stop moving even after only 5 min exposure to Hg^{2+}. Pt-Cat microrobots showed efficient removal of Hg^{2+} ions after 5 and 30 min, which indicates the ability of microrobots to adsorb Hg^{2+} ions. Furthermore, Langmuir and Freundlich models were used in order to describe adsorption parameters. The linear form of Langmuir model describes relation between adsorbed Hg^{2+} and equilibrium concentration of microrobots solution

$$\frac{1}{q_e} = \frac{1}{Q_o} + \frac{1}{Q_o K_l C_e} \tag{3}$$

where Q_o (mg g^{-1}) is maximum adsorption coverage capacity for monolayer when saturation is reached, and K_l (dm^3 mg^{-1}) is Langmuir constant which quantifies affinity between Pt-pollen microrobots and Hg^{2+} ions.

Freundlich exponential equation is given by the following equation

$$\ln q_e = \ln K_f + \frac{1}{n} \ln C_e \tag{4}$$

where q_e (mg g^{-1}) is the adsorption capacity at equilibrium, K_f and n are Freundlich dimensionless isotherm constants which represent adsorption capacity and adsorption intensity,

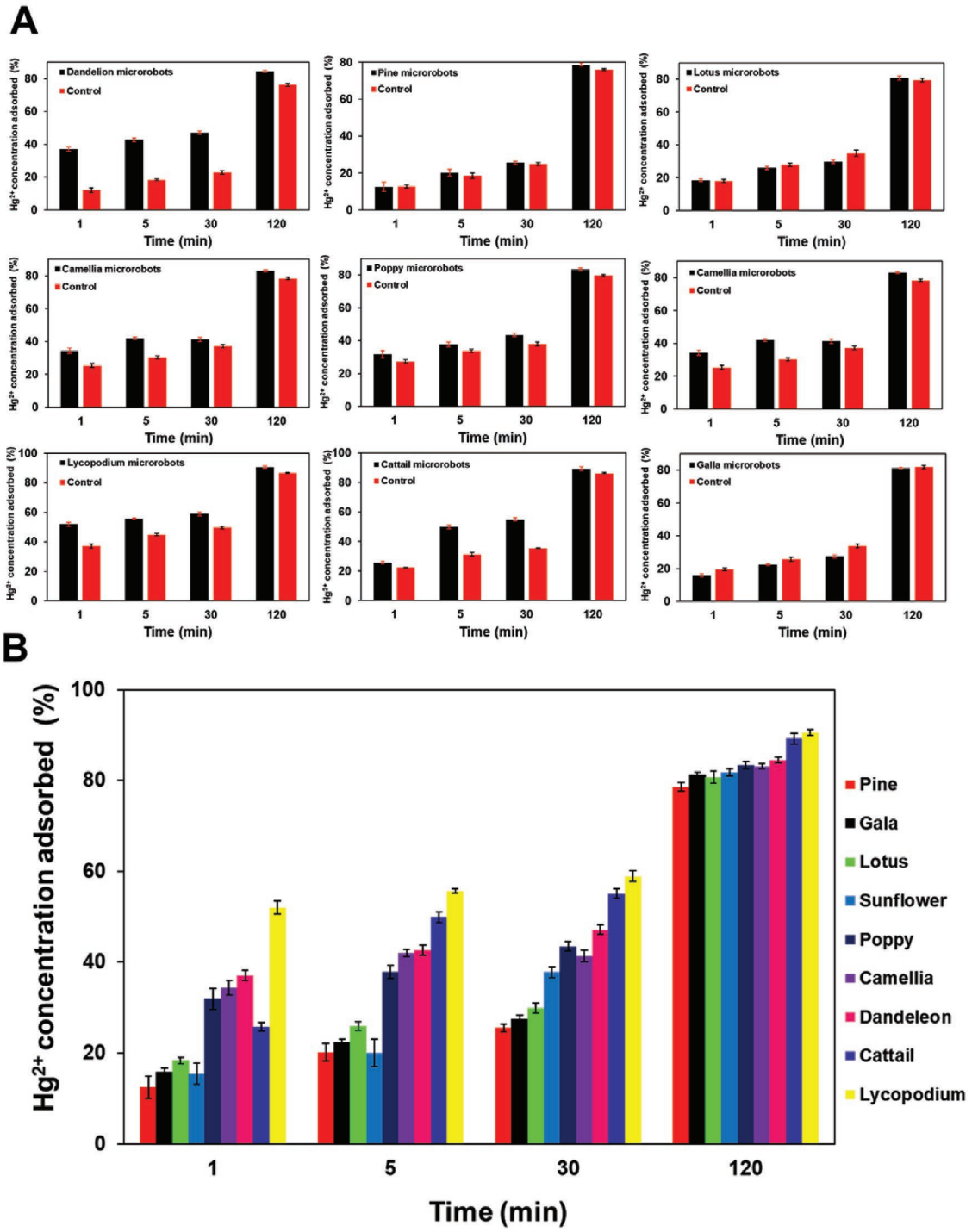

Figure 4. A) Influence of exposure time on Hg^{2+} removal by Pt-pollen microrobots (black bars) and corresponding bare pollen grains (red bars). B) Comparative analysis of Hg^{2+} adsorption of all fabricated Pt-pollen microrobots at different exposure times over duration of 120 min. Error bars represent standard deviations from three independent measurements.

respectively, and C_e (mg L^{-1}) is the equilibrium time concentration of Hg^{2+} in microrobots solution.

Experimental data obtained for Langmuir and Freundlich models are presented in Table S1 in the Supporting Information. Adsorption and correlation coefficients presented in Table S1 in the Supporting Information were calculated from Langmuir (Figure S1, Supporting Information) and Freundlich (Figure S2, Supporting Information) isotherms plots for Hg^{2+} adsorption onto Pt-pollen microrobots. As observed from Table S1 in the Supporting Information, better approximations to experimental values were obtained with Langmuir equation for all prepared microrobots except for Pt-Pop microrobots where

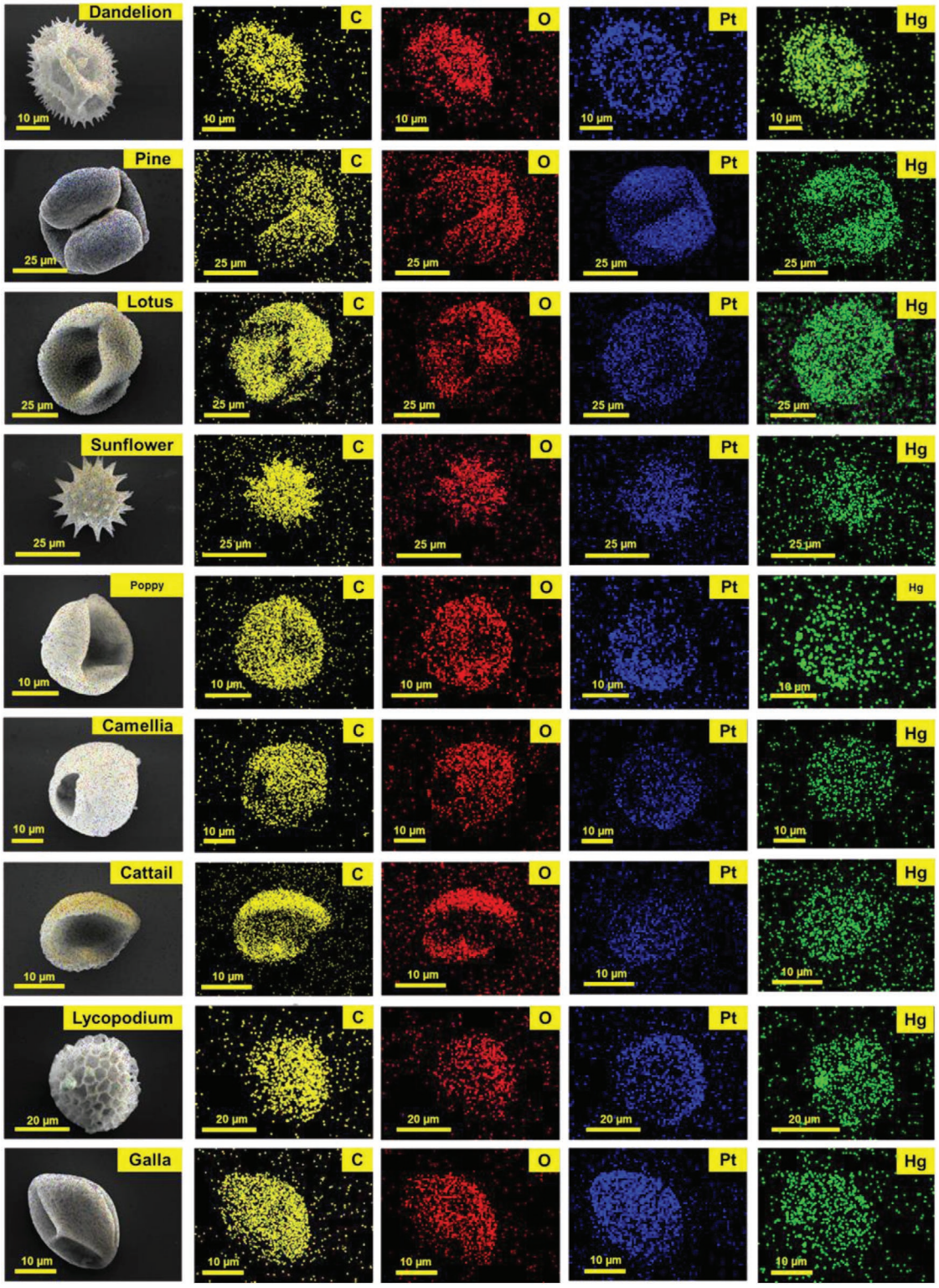

Figure 5. SEM images and corresponding EDS elemental mappings of respective fabricated Pt-pollen microrobots after adsorption of Hg^{2+} illustrating the distribution of C, O, Pt, and Hg. Scales as indicated in respective images.

experimental data fit better with Freundlich equation. Particularly, the correlation coefficient for Pt-Pop microrobots show better mathematical fit with Freundlich equation ($R^2 \approx 0.993$) compared to Langmuir equation ($R^2 \approx 0.989$). This would indicate the heterogenous adsorption surface of Pt-Pop microrobots which is followed by interactions between adsorbed species.[54]

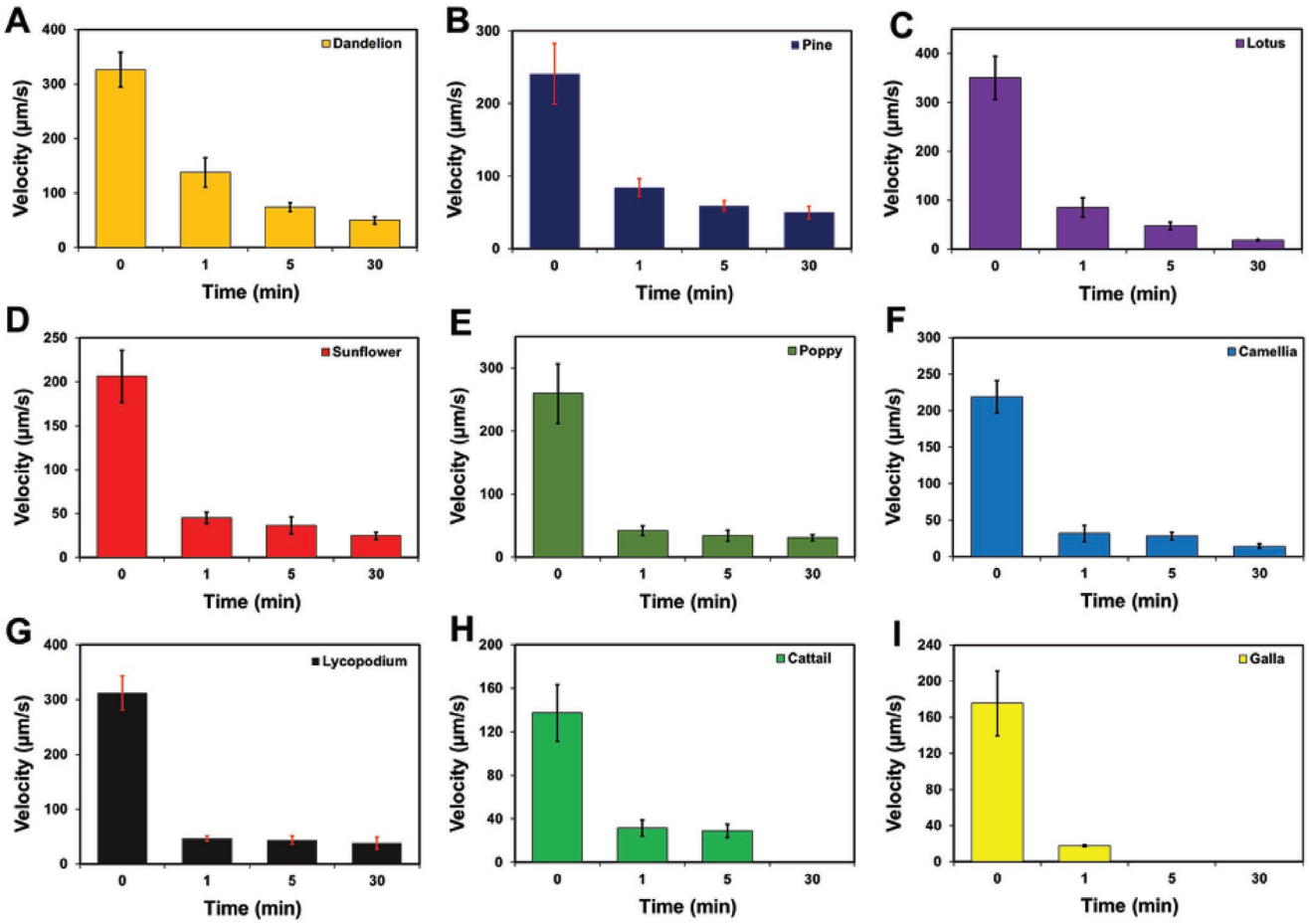

Figure 6. Average velocities of fabricated Pt-pollen microrobots at different time intervals over duration of 30 min in the presence of 1 ppm Hg^{2+}.

As the $1/n$ is greater than 1 ($1/n \approx 1.223$ for Pt-Pop microrobots), it would indicate that bonding energy decreases with surface density. Taking into account that Langmuir model takes into account that adsorption takes place on homogenous sites of the microrobots,[55] adsorption of Hg^{2+} ions occurs on the homogenous surface of Pt-pollen microrobots by forming monolayer with the exception of Pt-Pol microrobots.

Additionally, we set effort to investigate the potential application of Pt-pollen microrobots in biomedicine. It would thus be of fundamental importance to perform cytotoxicity assessments of the fabricated microrobots. Bianko previously reported that shape, size, generation of oxygen reactive particles, and morphological properties of the nanomaterials influenced their toxicological profiles.[56] As such, it was postulated that there would be minimal differences in toxicities between the fabricated microrobots. The fabricated microrobots were also expected to display low toxicities due to the natural availability and intrinsic nature of the pollen grains. Human breast cancer cells (MCF-7) were used in the cytotoxicity assessments of all nine fabricated Pt-pollen microrobots as breast cancer is the most commonly diagnosed cancer among females and accounts for 14% of total death from cancer.[57] MCF-7 cell line is widely used in research and represents an essential model for molecular analysis in breast cancer research.[58] In vitro cytotoxicity experiments were carried out by investigating cell viability of MCF-7 cells after 24 h exposure to different concentrations of the respective fabricated microrobots and the toxicological profiles are presented in **Figure 7**. Negative and positive control experiments were performed in the absence of microrobots and presence of 10% dimethyl sulfoxide (DMSO), respectively. Water-soluble tetrazolium salt (WST-8) cell viability assay was used to measure cell viabilities. Bars labeled as "0" correspond to the highest (initial) concentration of microrobots without dilution while bars presented with dilution factor "16" represent the smallest concentration of microrobots. All data presented in Figure 7 do not indicate concentration-dependence toxicity on MCF-7 cells viability. The results obtained show that more than 70% of MCF-7 cells remained viable after introduction of the highest concentration of each fabricated microrobot. Cell viability did not change drastically upon introduction of the most diluted microrobots solution. In contrast, cell viability was dropped by 88% upon addition of positive control (10% DMSO). These results affirm the nontoxic profile of each fabricated microrobots. All external interferences derived from WST-8 assay and microrobots were removed by subtracting from control experiments. However, the plot shows strong variations in cell viability between different pollen grains (consistent throughout all concentrations) which is understandably taking account of their different shape,

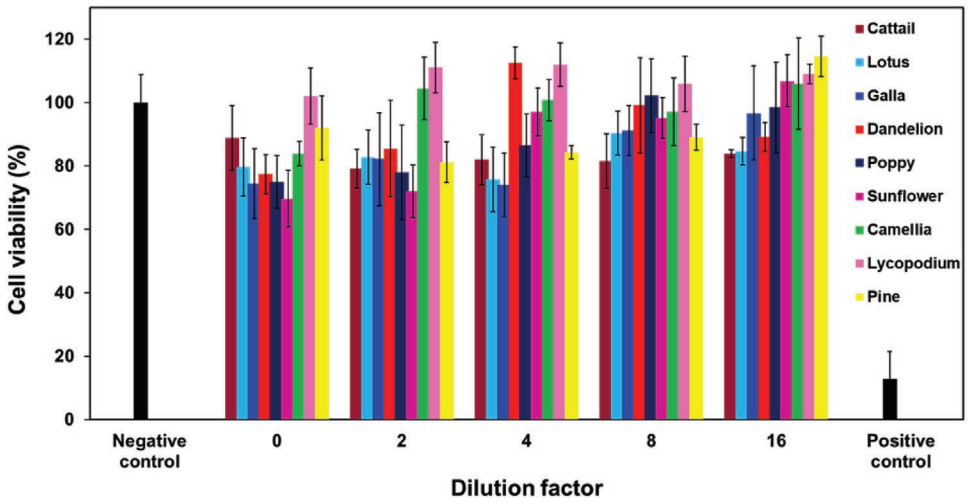

Figure 7. Cell viability percentages of different Pt-pollen microrobots at different dilution factors incubated with MCF-7 breast cancer cells for 24 h measured using WST-8 assay. Negative and positive experiments are displayed for comparison. The concentrations that were tested ranges from 100 to 6.25 μg mL^{-1}.

size, morphology, and structure. Different pollen grains realize different type of pollen proteins which may destruct intercellular contact proteins by proteolytic actions.[59,60]

Statistical analysis of significant work claims is provided in Table S1 in the Supporting Information for better comparison. Having verified the nontoxic nature of the fabricated Pt-pollen microrobots, we further explored and evaluated their potential application as drug carriers. Previous studies showed that pollen grains has great potential to be delivery agent for different drugs.[61–63] Loading of cargo onto the mobile Pt-pollen microrobots would potentially allow for targeted delivery and release to specified target locations in the human body. With this in mind, we decided to investigate the possibility of loading anti-cancer drug Doxorubicin (DOX) onto the fabricated Pt-Lot microrobots. Pt-Lot microrobots were chosen as the representative microrobots due to their desirable large size and great mobility. Their high surface area makes them more suitable for large quantities drug loading than smaller Pt-pollen micromotors. According to the results presented in Figure 6 where velocity of Pt-pollen microrobots is drastically reduced in the presence of Hg^{2+} ions, it can be expected that velocity of Pt-Lot microrobots reduces after drug loading as well. Taking into account that microrobots should meet biological safety requirements, only small concentration (10×10^{-6} M) of H_2O_2 can be used.[64,65] Figure 3A exhibits very high average velocity of Pt-Lot microrobots in the both 3% and 5% H_2O_2 so those microrobots have more chance to be propelled in the presence of 10×10^{-6} M of H_2O_2 (even with small velocity, Supporting Information Note S1) compared to other prepared microrobots. DOX is known to be fluorescently active in the red light spectrum (excitation wavelength: 560–570 nm). Bare Pt-Lot microrobots did not exhibit fluorescence at the specific excitation wavelength as predicted (**Figure 8**B). Pt-Lot microrobots with bounded DOX (DOX-Pt-Lot; Figure 8D) gave apparent fluorescence which suggested the successful attachment of DOX onto the surface of Pt-Lot microrobots. Hydroquinone group on DOX molecules could bind onto the sputtered Pt surface of Pt-Lot microrobots.[66] The Pt-Lot microrobots were thoroughly washed prior to fluorescence measurements to remove interferences from the unbounded DOX molecules to avoid negative results. Additionally, upon comparison of the optical images between bare and DOX-Pt-Lot microrobots (Figures 8A,C), there did appear to be any noticeable differences in the structures of the microrobots which would suggest that DOX molecules did not drastically affect the structural integrity of the microrobots. Having determined the successful loading of DOX onto the fabricated microrobots, it is imperative to investigate the contribution of Pt-Lot microrobots toward the delivery of drugs to target cancer cells via in vitro cytotoxicity assessments using MCF-7 cell line. From Figure 8E, both bare lotus pollen grains Pt-Lot microrobots did not exhibit any toxicity toward MCF-7 cells. However, introduction of DOX onto Pt-Lot microrobots in the presence of 1% SDS and 3% H_2O_2 resulted in the significant decrease in cell viability to 41%. This is almost comparable to free-moving DOX (positive control) which caused cell viability to drop to ≈23%. The results obtained indicate enhanced efficiency of Pt-Lot microrobots for DOX delivery to cancerous cells. Pollen grains can potentially be functionalized and fabricated into microrobots to be used in medical applications for noninvasive transport and delivery of drugs to targeted locations effectively.

3. Conclusion

We have successfully fabricated microrobots derived from natural pollen grains for environmental remediation and biomedical applications. Pollen grains (cattail, lotus, galla, dandelion, poppy, sunflower, camellia, lycopodium, and pine) incorporated with Pt exhibited an excellent approach toward fabrication of microrobots in large quantities. The results demonstrated excellent microrobots propulsion by bubbles formation from the decomposition of hydrogen peroxide fuel. It was also found that Pt-pollen microrobots exhibit great adsorption toward Hg^{2+} ions in aqueous solution. Maximum adsorption efficiency of all fabricated microrobots was achieved 120 min after exposure to 1 ppm Hg^{2+} (>80%). The velocities of the fabricated microrobots

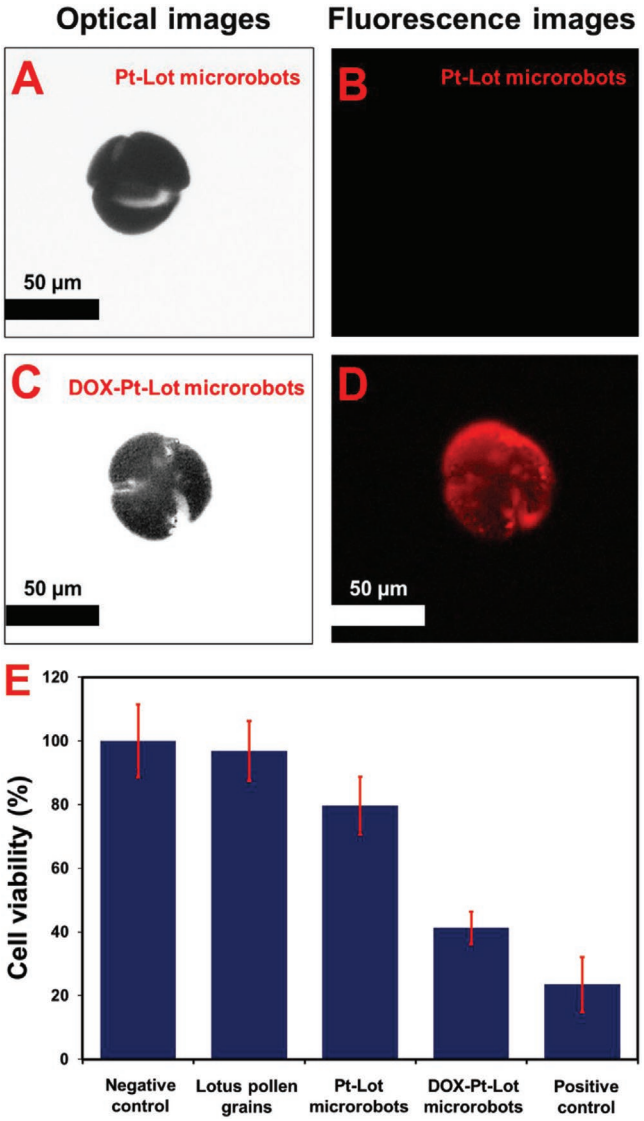

Figure 8. A) Optical and B) fluorescence images of Pt-pollen microrobots. C) Optical and D) fluorescence images of DOX-loaded Pt-pollen microrobots. E) Cell viability results of MCF-7 cells for negative control (WST-8 assay), bare Lotus pollen, Pt-pollen microrobots, DOX-loaded Pt-pollen microrobots, and positive control (10% DOX). Incubation time of 120 min. Error bars represent standard deviations for each parameter.

decreased significantly in the presence of 1 ppm Hg^{2+} during the experimental duration. The fabricated microrobots were found to be nontoxic from cytotoxicity assessments which expand their potential use in biomedicine and drug loading. Additionally, Pt-pollen microrobots were found to be efficient carriers of Doxorubicin (DOX) drug which opens potentiality to be transported to target sites throughout the body.

4. Experimental Section

Materials: Defatted pollen grains from sunflower (*Helianthus annuus* L.), pine (*Pinus taeda*), and dandelion (*Taraxacum officinale*) families were purchased from Greer Laboratories, Inc. (Lenoir, NC). Lycopodium (*Lycopodium clavatum*) spores (S-type) and cattail (*Typhae angustfolia*) pollen grains were purchased from Sigma-Aldrich (St. Louis, MO). Camellia (*Camellia Sinensis* L.) bee pollen granules were purchased from Yuensun Biological Technology Co., Ltd. (Xi'an, Shaanxi, China). Lotus (*Nelumbo nucifera*) and poppy (*Papaver rhoeas*) pollens were purchased from Peffer Industrial Co., Ltd. (Zhengzhou, Henan, China). Hydrogen peroxide (H_2O_2, 35 wt%) was obtained from Alfa Aesar (Singapore). SDS, 3-(4,5-dimethylthiazol-2-yl)-2,5-diphenyltetrazolium bromide assay reagent, and mercuric nitrate monohydrate ($Hg(NO_3)_2$ x H_2O) were purchased from Sigma-Aldrich (Singapore). Water-soluble tetrazolium salt (WST-8) assay reagent was supplied by Dojindo. Phosphate buffer solution (PBS), fetal bovine serum (FBS), Dulbecco's modified Eagle medium (DMEM), and penicillin-streptomycin liquid (1%) were purchased from Gibco. Trypsin was obtained from Life Technologies (Singapore).

Instruments: Microrobots structure characterization was obtained by JEOL 7600F (Jeol, Japan) at an accelerating voltage of 5 kV for SEM and accelerating voltage of 15 kV for EDS, respectively. Absorbance readings were performed using Thermo Multiskan GO (Thermo Fisher Scientific). DIPA was performed by FlowCam (Fluid Imaging Technologies, Maine, USA). Sputtering machine (JEOL JFC-1600 Auto Fine Coater) was used for Pt coating onto the respective plant pollens. Optical microscope (Nicon Eclipse TE 2000-E) connected to Nikon NIS-Elements software was employed to perform velocity measurements. Concentrations of Hg^{2+} were obtained with inductively coupled plasmamass spectrometry (Agilent 7700 Series, Japan). Drug-loaded Pt-pollen microrobots fluorescence images were captured by an optical microscope coupled with filter (excitation wavelength: 560–570 nm).

Pollen Grains Preparation: Details of the fabrication of defatted pollen grains for various species are given in a recent study.[67] Briefly, 250 g of bee pollen granules were first 27 refluxed in 0.5 L of acetone in a round bottom flask under magnetic 28 stirring (50 °C, 220 rpm) for 3 h. Thereafter, acetone was decanted and sample was mixed with 1 L of deionized water for 1 h. Subsequently, pollen suspension was filtrated through a 300 µm diameter pores nylon mesh and 6 µm diameter pores filter paper. 1 L deionized water was used to hydrate pollen sample for 30 min under magnetic stirring and subsequently filtered. First procedure was repeated: resulting sample was refluxed again in 500 mL of acetone under magnetic stirring (3 h, 400 rpm). Thereafter, acetone was removed with vacuum filtration and sample was stored in glass petri dish in a fume hood for 1 day. 250 mL of diethyl ether was mixed with 20 g of dried sample and stirred for 120 min (400 rpm, 25 °C). After repetition of last step twice, diethyl ether was removed by vacuum filter. Next, freshly used diethyl ether was mixed with pollen sample and left to stir overnight. Lastly, pollen sample was separated from diethyl ether, transferred to petri dish, and left to dry for 12 h in a fume hood.

Fabrication and Operation of Pt-Pollen Microrobots: All nine different types of Pt-pollen microrobots were prepared by the following procedures. 1 mg of respective plant pollen was suspended in 1 mL Milli-Q water and sonicated for 1 h. The solution was then dropped onto a glass slide (previously cleaned with ethanol) and left to dry overnight. Pt was then asymmetrically sputtered onto one side (t = 200 s, I = 40 mA). Subsequently, glass slide was ultrasonicated for about 30 s to detach the fabricated microrobots from the glass slide. The released microrobots were stored in distilled water.

Motion studies of microrobots were performed in solution which contains water, hydrogen peroxide (fuel), and SDS (surfactant). Average velocities of microrobots were calculated by measuring 20 individual velocities of the microrobots using an optical microscope.

Cytotoxicity Assessments: MCF-7 breast cancer cell line (Bio-REV Singapore) was used to determine cytotoxicity of the Pt-pollen microrobots. The cells were prepared in a medium consisting of DMEM, 10% FBS, and antibiotics (1% penicillin-streptomycin) in an incubator (conditions: 37 °C, 5% CO_2). The cells were seeded and grown in 96-well plates (5000 cells per well in 100 µL) for 24 h. Thereafter, medium was replaced with 100 µL of different dilutions of Pt-pollen microrobots suspensions in each well. Negative control experiments were performed with cells in the absence of fabricated microrobots while positive control experiments were performed in 10% DMSO. Subsequently, cells and

microrobots were incubated for 24 h (conditions: 37 °C, 5% CO_2). 10 µL of WST-8 reagent was introduced into each well and incubated for 1 h in wrapped aluminium foil. Lastly, absorbance was measured at excitation wavelength of 450 nm.

Quantification of Hg^{2+} Removed: Mercury ions adsorption studies were carried out in 500 µL of final solution. Concentration of pollen grains, SDS, and hydrogen peroxide was 0.5 mg mL^{-1}, 1%, and 4%, respectively. 1 ppm of mercury ions was added into the solution for different durations of 1, 5, 30, and 120 min. At the end of the respective exposure times, filtration (filter membrane 3 µm pore size) was performed to remove the microrobots from solution and the filtrate was obtained. Concentrations of Hg^{2+} remaining in filtrate were obtained using inductively coupled plasma-mass spectrometer. Percentage removal of Hg^{2+} by microrobots/bare pollen grains was calculated from the difference between initial concentration (1 ppm) and measured concentrations of filtrate at different exposure times. Three experiments were repeated for the same remediation time and conditions.

Loading of Doxorubicin (DOX) onto Pt-Pollen Microrobots: 1 mL suspension of Pt-pollen microrobots was dispersed in 28×10^6 M Doxorubicin solution (DOX) and left for 24 h. The mixture was centrifuged (12 000 rpm, 5 min) to remove free and unloaded DOX molecules in the solution. Cleaning procedure was repeated twice more. DOX-loaded Pt-pollen microrobots were finally resuspended in distilled water and used directly for fluorescence imaging.

Supporting Information

Supporting Information is available from the Wiley Online Library or from the author.

Acknowledgements

M.P. acknowledges financial support of the project Advanced Functional Nanorobots (Reg. No. CZ.02.1.01/0.0/0.0/15_003/0000444 financed by the EFRR). The authors acknowledge financial support from A*STAR grant (No. SERC A1783c0005), Singapore.

Conflict of Interest

The authors declare no conflict of interest.

Keywords

Doxorubicin, drug loading, environment remediation, micromotors, pollen grain

Received: January 6, 2020
Revised: February 17, 2020
Published online:

[1] L. Soler, V. Magdanz, V. M. Fomin, S. Sanchez, O. G. Schmidt, *ACS Nano* **2013**, *7*, 9611.
[2] M. Guix, C. C. Mayorga-Martinez, A. Merkoçi, *Chem. Rev.* **2014**, *114*, 6285.
[3] X. Lin, Z. Wu, Y. Wu, M. Xuan, Q. He, *Adv. Mater.* **2016**, *28*, 1060.
[4] I. Ortiz-Rivera, M. Mathesh, D. A. Wilson, *Acc. Chem. Res.* **2018**, *51*, 1891.
[5] I. Santiago, *Nano Today* **2018**, *19*, 11.
[6] M. Xuan, J. Shao, C. Gao, W. Wang, L. Dai, Q. He, *Angew. Chem., Int. Ed.* **2018**, *57*, 12463.
[7] L. F. Valadares, Y. G. Tao, N. S. Zacharia, V. Kitaev, F. Galembeck, R. Kapral, G. A. Ozin, *Small* **2010**, *6*, 565.
[8] S. Wang, N. Wu, *Langmuir* **2014**, *30*, 3477.
[9] J. P. Hernandez-ortiz, C. G. Stoltz, M. D. Graham, *Phys. Rev. Lett.* **2005**, *95*, 204501.
[10] M. Manjare, F. Yang, R. Qiao, Y. Zhao, *J. Phys. Chem. C* **2015**, *119*, 28361.
[11] D. Vilela, J. Parmar, Y. Zeng, Y. Zhao, S. Sánchez, *Nano Lett.* **2016**, *16*, 2860.
[12] D. A. Uygun, B. Jurado-Sánchez, M. Uygun, J. Wang, *Environ. Sci.: Nano* **2016**, *3*, 559.
[13] M. Guix, J. Orozco, M. Garcia, W. Gao, S. Sattayasamitsathit, A. Merkoči, A. Escarpa, J. Wang, *ACS Nano* **2012**, *6*, 4445.
[14] F. Mou, D. Pan, C. Chen, Y. Gao, L. Xu, J. Guan, *Adv. Funct. Mater.* **2015**, *25*, 6173.
[15] J. Parmar, D. Vilela, K. Villa, J. Wang, S. Sánchez, *J. Am. Chem. Soc.* **2018**, *140*, 9317.
[16] R. Dong, Q. Zhang, W. Gao, A. Pei, B. Ren, *ACS Nano* **2016**, *10*, 839.
[17] S. Sattayasamitsathit, K. Kaufmann, M. Galarnyk, R. Vazquez-Duhalt, J. Wang, *RSC Adv.* **2014**, *4*, 27565.
[18] J. Orozco, D. Vilela, G. Valdés-Ramírez, Y. Fedorak, A. Escarpa, R. Vazquez-Duhalt, J. Wang, *Chem. - Eur. J.* **2014**, *20*, 2866.
[19] S. Campuzano, J. Orozco, D. Kagan, M. Guix, W. Gao, S. Sattayasamitsathit, J. C. Claussen, A. Merkoçi, J. Wang, *Nano Lett.* **2012**, *12*, 396.
[20] Y. Tu, F. Peng, A. A. M. André, Y. Men, M. Srinivas, D. A. Wilson, *ACS Nano* **2017**, *11*, 1957.
[21] J. Chen, S. Ratnayaka, A. Alford, V. Kozlovskaya, F. Liu, B. Xue, K. Hoyt, E. Kharlampieva, *ACS Nano* **2017**, *11*, 3135.
[22] M. N. Centelles, M. Wright, P. W. So, M. Amrahli, X. Y. Xu, J. Stebbing, A. D. Miller, W. Gedroyc, M. Thanou, *J. Controlled Release* **2018**, *280*, 87.
[23] S. K. Srivastava, M. Medina-Sánchez, B. Koch, O. G. Schmidt, *Adv. Mater.* **2016**, *28*, 832.
[24] W. Gao, B. E. F. de Ávila, L. Zhang, J. Wang, *Adv. Drug Delivery Rev.* **2018**, *125*, 94.
[25] M. Uygun, B. Jurado-Sánchez, D. A. Uygun, V. V. Singh, L. Zhang, J. Wang, *Nanoscale* **2017**, *9*, 18423.
[26] J. Shao, M. Xuan, L. Dai, T. Si, J. Li, Q. He, *Angew. Chem., Int. Ed.* **2015**, *54*, 12782.
[27] W. Montgomery, C. Potiszil, J. S. Watson, M. A. Sephton, *Macromol. Chem. Phys.* **2016**, *217*, 2494.
[28] G. Mackenzie, A. N. Boa, A. Diego-Taboada, S. L. Atkin, T. Sathyapalan, *Front. Mater.* **2015**, *2*, 66.
[29] C. Chiappe, G. C. Demontis, V. Di Bussolo, M. J. Rodriguez Douton, F. Rossella, C. S. Pomelli, S. Sartini, S. Caporali, *Green Chem.* **2017**, *19*, 1028.
[30] C. Hu, H. Vogler, M. Aellen, N. Shamsudhin, B. Jang, J. T. Burri, N. Laubli, U. Grossniklaus, S. Pane, B. J. Nelson, *Lab Chip* **2017**, *17*, 671.
[31] A. K. Prabhakar, H. Y. Lai, M. G. Potroz, M. K. Corliss, J. H. Park, R. C. Mundargi, D. Cho, S. I. Bang, N. J. Cho, *J. Ind. Eng. Chem.* **2017**, *53*, 37.
[32] R. P. Wodehouse, *J. Nerv. Ment. Dis.* **1937**, *86*, 104.
[33] P. Piffanelli, J. H. Ross, D. J. Murphy, *Sex. Plant Reprod.* **1998**, *11*, 65.
[34] a) P. B. Tomlinson, M. M. Harley, C. M. Morton, S. Blackmore, in *Pollen and Spores: Morphology and Biology* (Eds: M. M. Harley, C. M. Morton, S. Blackmore), Royal Botanic Gardens, Kew **2000**, p. 147; b) W. Punt, P. P. Hoen, S. Blackmore, S. Nilsson, A. L. Thomas, *Rev. Palaeobot. Palynol.* **2007**, *143*, 1.
[35] E. Domínguez, J. A. Mercado, M. A. Quesada, A. Heredia, *Sex. Plant Reprod.* **1999**, *12*, 171.

[36] T. Fan, J. H. Park, Q. A. Pham, E. L. Tan, R. C. Mundargi, M. G. Potroz, H. Jung, N. J. Cho, *Sci. Rep.* **2018**, *8*, 6565.
[37] A. K. Prabhakar, M. G. Potroz, S. Park, E. Miyako, N. J. Cho, *Part. Part. Syst. Charact.* **2018**, *35*, 1800151.
[38] A. K. Prabhakar, M. G. Potroz, E. L. Tan, H. Jung, J. H. Park, N. J. Cho, *ACS Appl. Mater. Interfaces* **2018**, *10*, 28428.
[39] R. C. Mundargi, E. L. Tan, J. Seo, N. J. Cho, *J. Ind. Eng. Chem.* **2016**, *36*, 102.
[40] H. Wang, M. G. Potroz, J. A. Jackman, B. Khezri, T. Marić, N. J. Cho, M. Pumera, *Adv. Funct. Mater.* **2017**, *27*, 1702338.
[41] H. Wang, G. Zhao, M. Pumera, *J. Am. Chem. Soc.* **2014**, *136*, 2719.
[42] J. Wittborn, K. V. Rao, G. El-Ghazaly, J. R. Rowley, *Ann. Bot.* **1998**, *82*, 141.
[43] V. K. Thakur, M. K. Thakur, *Handbook of Polymers for Pharmaceutical Technologies*, Vol. *1*, Wiley, New York **2015**.
[44] M. Manjare, B. Yang, Y. P. Zhao, *Phys. Rev. Lett.* **2012**, *109*, 128305.
[45] W. Huang, M. Manjare, Y. Zhao, *J. Phys. Chem. C* **2013**, *117*, 21590.
[46] N. H. Fletcher, *J. Chem. Phys.* **1958**, *29*, 572.
[47] J. S. McNown, J. Malaika, *EOS, Trans., Am. Geophys. Union* **1950**, *31*, 74.
[48] R. Maria-Hormigos, B. Jurado-Sanchez, L. Vazquez, A. Escarpa, *Chem. Mater.* **2016**, *28*, 8962.
[49] J. Neustadt, S. Pieczenik, *Integr. Med.* **2007**, *6*, 36.
[50] H. Ali, E. Khan, M. A. Sajad, *Chemosphere* **2013**, *91*, 869.
[51] T. Maric, C. C. Mayorga-Martinez, B. Khezri, M. Z. M. Nasir, X. Chia, M. Pumera, *Adv. Funct. Mater.* **2018**, *28*, 1802762.
[52] T. Maric, C. C. Mayorga-Martinez, M. Z. M. Nasir, M. Pumera, *Adv. Mater. Technol.* **2018**, *4*, 1800502.
[53] J. Salter, B. G. Murray, J. E. Braggins, *Ann. Bot.* **2002**, *89*, 133.
[54] H. M. F. Freundlich, *J. Phys. Chem.* **1906**, *57*, 1100.
[55] I. Langmuir, *J. Am. Chem. Soc.* **1918**, *40*, 1361.
[56] A. Bianco, *Angew. Chem., Int. Ed.* **2013**, *52*, 4986.
[57] Ş. Comşa, A. M. Cîmpean, M. Raica, *Int. J. Cancer Res. Treat.* **2015**, *35*, 3147.
[58] S. E. Burdall, A. M. Hanby, M. R. J. Lansdown, V. Speirs, *Breast Cancer Res.* **2003**, *5*, 89.
[59] D. F. Rabensteiner, J. Rabensteiner, J. Horwath-Winter, D. Lang-Loidolt, A. Wedrich, A. Heidinger, G. Schwantzer, O. Schmut, *Cutaneous Ocul. Toxicol.* **2019**, *38*, 93.
[60] S. Runswick, T. Mitchell, P. Davies, C. Robinson, D. R. Garrod, *Respirology* **2007**, *12*, 834.
[61] S. L. Atkin, S. Barrier, S. T. Beckett, T. Brown, G. Mackenzie, L. Madden, *Collect. Czech. Chem. Commun.* **2015**, *7*, 307.
[62] L. Akyuz, I. Sargin, M. Kaya, T. Ceter, I. Akata, *Mater. Sci. Eng. C* **2017**, *71*, 937.
[63] V. N. Paunov, G. Mackenzie, S. D. Stoyanov, *J. Mater. Chem.* **2007**, *17*, 609.
[64] K. J. Davies, *IUBMB Life* **1999**, *48*, 41.
[65] B. Halliwell, M. V. Clement, L. H. Long, *FEBS Lett.* **2000**, *486*, 10.
[66] F. Zunino, G. Savi, A. Pasini, *Cancer Chemother. Pharmacol.* **1986**, *18*, 180.
[67] T.-F. Fan, S. Park, Q. Shi, X. Zhang, Q. Liu, Y. Song, H. Chin, M. S. B. Ibrahim, N. Mokrzecka, Y. Yang, H. Li, J. Song, S. Suresh, N.-J. Cho, *Nat. Commun.* **2020**, in press.